


## Orthogonal Thermal Noise and Transmission Signals: A New Coherent Perfect Absorption's Feature

Douglas Oña<sup>✉</sup>, Angel Ortega-Gomez, Osmerly Hernández<sup>✉</sup>, and Iñigo Liberal<sup>✉\*</sup>  
*Department of Electrical, Electronic, and Communications Engineering, Institute of Smart Cities (ISC),  
Public University of Navarre (UPNA), 31006 Pamplona, Spain*

 (Received 27 November 2023; accepted 5 August 2024; published 6 September 2024)

Coherent perfect absorption (CPA) is an interference process associated with the zeros of the scattering matrix of interest for optical computing, data processing, and sensing. However, the noise properties of CPA remain relatively unexplored. Here, we demonstrate that CPA thermal noise signals exhibit a unique property: they are orthogonal to the signals transmitted through the network. In turn, such property enables a variety of thermal noise management effects, such as the physical separability of thermal noise and transmitted signals, and “externally lossless” networks that internally host radiative heat transfer processes. We believe that our results provide a new perspective on the many CPA technologies currently under development.

DOI: [10.1103/PhysRevLett.133.103801](https://doi.org/10.1103/PhysRevLett.133.103801)

Coherent perfect absorption (CPA) is an interference process in which the coherent processes of one or more signals cancels all output signals, resulting in complete absorption [1–3]. CPA can also be interpreted as the time-reversed process of lasing as threshold [1], where the signals are outgoing rather than ingoing, and where the poles of  $\mathbf{S}$  are moved upward onto the real axis by the addition of gain [4]. Importantly, CPA should not be confused with the more general effect of reflectionless scattering modes (RSMs) [5,6], as CPA explicitly requires that all energy missing in the system is irreversibly lost to heat, while RSMs do not. Despite this critical distinction, we note the RSM experimental setups can be converted to CPA if the additional electromagnetic outgoing modes are terminated in a matched load or perfect absorber, bringing at the same time a modification in the resulting configuration. Both CPA and RSMs are very general phenomena that apply to systems with strong mode overlap [7].

CPA and the more general RSMs have been experimentally demonstrated in multiple configurations, including planar slabs [8], metasurfaces [9], graphene layers [10], integrated photonics [11–14], surface plasmon polariton gratings [15], and epsilon-near-zero media [16]. CPA in the single photon regime has been observed with plasmonic metasurfaces [17–20]. Recently, CPA and RSMs have been demonstrated in the context of disordered media [21], resonators supporting exceptional points [22], chaotic RSMs in resonators supporting thousands of resonances [5,23–25], and optical cavities with massively degenerated CPA modes [26]. On the other hand, precise control of CPA modes has also been facilitated by the use of reconfigurable

metasurfaces [27–30]. Beyond optical systems, CPA has been demonstrated with matter [31] and sound [32] waves.

When CPA is based on more than one signal, it effectively enables light-with-light interactions in a linear system [2]. Thus, it finds natural applications in interferometry [8], all-optical data processing [33,34], sensing, as well as in photocurrent generation [35] and photoluminescence [36].

Here, we theoretically demonstrate that CPA modes enable orthogonal channels for thermal noise and transmission signals. We find that because of the algebraic properties of CPA modes, the heat radiated by an optical network and the signals transmitted through it occupy orthogonal vector spaces. The same property allows for the internal exchange of heat within an optical network, while simultaneously confining all thermal signals within the network and remaining transparent to all their input optical modes. We believe these results bring a fresh perspective to the physics of CPA, and it could be applied to the many CPA technologies that are currently under investigation [1–4,8–23,26,31–38]. We note that previous works on the quantum optical response of CPA devices include noise operators [19,39,40], from which thermal emission could be derived. However, such works focus on the photon statistics of nonclassical light states, while the thermal emission emanating from them has received less attention. In addition, infrared thermal radiation is key for heat and energy management applications [41], thermal imaging [42,43], and camouflage [44,45], as well as gas sensing [46,47].

To guide our thoughts, we consider an optical network with  $M$  left and  $N$  right ports, with  $N > M$  [see Fig. 1(a)]. We assume that all ports are matched, so that there are no back reflections. As we will show, our results actually apply

\*Contact author: [inigo.liberal@unavarra.es](mailto:inigo.liberal@unavarra.es)

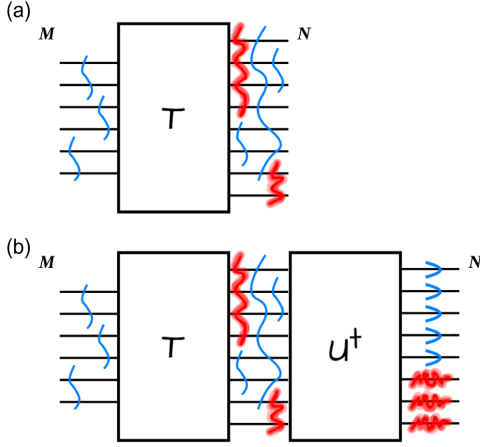


FIG. 1. (a) Schematic of a network of  $M$  left ports and  $N$  right ports. The glowing redlines are the thermal noise signals exiting the network, while the blue lines represent the signals transmitted through it. (b) Physical separation of the CPA thermal noise (red) and the transmitted signals (blue) by means of a unitary network, resulting in each algebraic output mode being assigned to a physical port.

to arbitrary networks (see Supplemental Material [48]). However, this configuration has two benefits: (a) outgoing signals appear as signals transmitted through the network from left to right, which are easier to visualize; and (b) input and outgoing signals appear on physically different channels and can be processed without using a full duplex detector. The vectors of input and output signals,  $\mathbf{a}$  and  $\mathbf{b}$  respectively, are related through a  $\mathbf{S} \in \mathbb{C}^{(M+N) \times (M+N)}$  scattering matrix  $\mathbf{b} = \mathbf{S}\mathbf{a}$ . We label the  $M + N$  ports such that the first  $M$  ports correspond to the ports on the left side of the network, while the subsequent  $N$  ports are the ports on the right (see Supplemental Material). Then, if all input ports are matched and the network is reciprocal, the scattering matrix can be written as follows:

$$\mathbf{S} = \begin{bmatrix} \mathbf{0}_{M \times M} & \mathbf{T}^T \\ \mathbf{T} & \mathbf{0}_{N \times N} \end{bmatrix}, \quad (1)$$

where  $\mathbf{T} \in \mathbb{C}^{N \times M}$  is the transmission matrix characterizing the left-to-right transmission of signals through the network. It is important to note that, for realistic systems, Eq. (1) can only be exactly satisfied at discrete frequencies, although an approximately similar behavior can be observed over a finite operational bandwidth (see Supplemental Material). For any linear network,  $\mathbf{T}$  admits a singular value decomposition (SVD) [20,49]  $\mathbf{T} = \mathbf{U}\mathbf{D}\mathbf{V}^\dagger$ , where  $\mathbf{U} \in \mathbb{C}^{N \times N}$  is a unitary matrix  $\mathbf{U}\mathbf{U}^\dagger = \mathbf{I}_N$  providing a basis for the signals outgoing the  $N$  ports on the right, and  $\mathbf{V} \in \mathbb{C}^{M \times M}$  is a unitary matrix  $\mathbf{V}\mathbf{V}^\dagger = \mathbf{I}_M$  providing a basis for the signals incoming through the  $M$  left ports.  $\mathbf{D} \in \mathbb{R}^{+N \times M}$  is a matrix of singular values with the following structure:

$$\mathbf{D} = \begin{bmatrix} \mathbf{D}_T \\ \cdots \\ \mathbf{0}_{(N-M) \times M} \end{bmatrix}, \quad (2)$$

with  $\mathbf{D}_T = \text{diag}\{d_1, \dots, d_M\}$  and  $d_n \in \mathbb{R}^+ \forall n$  are the singular values. It is also interesting to structure  $\mathbf{U}$  as

$$\mathbf{U} = [\mathbf{U}_T \quad \vdots \quad \mathbf{U}_0], \quad (3)$$

highlighting that while the columns of  $\mathbf{U}$  span the complete vectorial space in the right output ports, with dimension  $N$ , the transmission signals that can be excited from the left are restricted to the space spanned by the columns of  $\mathbf{U}_T \in \mathbb{C}^{N \times M}$  with dimension  $M$ . The space spanned by the columns of  $\mathbf{U}_0 \in \mathbb{C}^{N \times N-M}$  with dimension  $N - M$  are inaccessible to the signals. Inspecting the SVD of  $\mathbf{S}$  (see Supplemental Material) shows that these inaccessible  $N - M$  modes correspond to CPA modes when the system is excited with an input vector of dimension  $(M + N) \times 1$ , with the first  $M$  inputs equal to zero. This would be equivalent to exciting the  $N$  inputs of the system presented in Fig. 1(a). In addition, if any of the remaining singular values equal zero,  $d_n = 0$ , we would have additional CPA modes. In general, any reflectionless network with an asymmetric number of ports contains at least  $N - M$  channels that are inaccessible to the transmitted signals and the signal processing tasks performed by the network.

At the same time, any lossy network at temperature  $T$  emits thermal radiation, which can be modeled through  $n_n(\omega)$  stochastic signals exiting each port,  $n = 1, \dots, N + M$ . Thermal noise signals are assumed to be random, with no phase information and zero average  $\langle n_n(\omega) \rangle = 0 \forall n$ , frequency uncorrelated  $\langle n_n^*(\omega) n_m(\omega') \rangle = A_{nm} \delta(\omega - \omega') \forall n, m$ , and further characterized by the noise correlation matrix [50–52]

$$\langle \mathbf{nn}^\dagger \rangle = (\mathbf{I} - \mathbf{S}\mathbf{S}^\dagger) N_T, \quad (4)$$

where  $N_T = (1/2\pi) \hbar \omega (e^{\hbar\omega/k_B T} - 1)^{-1}$  is the black-body energy spectrum. Equation (4) implicitly assumes that the network is in thermal equilibrium at temperature  $T$ . Considering a device with parts at different temperatures would require local thermal equilibrium theories for thermal emission [53]. The diagonal elements of Eq. (4) describe the thermal noise power exiting each port, while the nondiagonal elements represent nontrivial correlations (spatial coherence) between the noise signals exiting different ports.

After a number of algebraic manipulations (see Supplemental Material), we find that the correlation matrix admits the following eigendecomposition

$$\langle \mathbf{nn}^\dagger \rangle = \mathbf{P}\mathbf{D}_N\mathbf{P}^\dagger N_T, \quad (5)$$

where  $\mathbf{P}\mathbf{P}^\dagger = \mathbf{I}_{N+M}$  is a unitary matrix, constructed from the  $\mathbf{V}$  and  $\mathbf{U}$  matrices as

$$\mathbf{P} = \begin{bmatrix} \mathbf{V}^* & \mathbf{0}_{M \times N} \\ \mathbf{0}_{N \times M} & \mathbf{U} \end{bmatrix} \quad (6)$$

and

$$\mathbf{D}_N = \text{diag}\{1 - d_1^2, \dots, 1 - d_M^2, 1 - d_1^2, \dots, 1 - d_M^2, \mathbf{1}_{1 \times N-M}\}. \quad (7)$$

The first  $2M$  diagonal entries in (7) show the existence of thermal signals for each  $n$ th channel for which  $d_n < 1$ . For these channels, the transmitted power is reduced by a factor  $d_n^2$ , while a  $(1 - d_n^2)N_T$  noise power is added into the channel. Thus, thermal noise and transmitted signals overlap in the same physical channel when  $d_n < 1$ , leading to known reduction of the SNR by a lossy device. On the other hand, the last  $N - M$  diagonal entries in (7) equal 1, meaning that the  $N - M$  CPA modes inaccessible to the transmitted signals also act as perfect blackbody thermal emitters. However, the additional noise introduced by CPA thermal signals occupies an orthogonal space to the space of transmitted signals. For a system in which  $d_n = 0 \forall n$ , all the thermal emission from the device and the transmitted signals would occupy orthogonal spaces. For channels in which  $d_n > 0$ , thermal noise signals are progressively less orthogonal to the transmitted signals, as the singular value deviates from zero. Therefore, it is a unique feature of CPA modes that thermal noise and transmitted signals are orthogonal. We note that this conclusion does not require any assumption on the network except from linearity, and it can be applied to arbitrary devices (see Supplemental Material). In fact, it can be applied to both reciprocal and nonreciprocal devices (see Supplemental Material).

*Physical separability*—A direct consequence from the fact that thermal CPA and transmitted signals occupy orthogonal channels is that they can be physically separated. Again, for a system with only either transparent or CPA channels, i.e.,  $d_n = 1 \forall n$ , all thermal noise and transmitted signals occupy orthogonal channels. Thus, if we change the basis of the thermal noise signals to  $\mathbf{n}_p = \mathbf{P}^\dagger \mathbf{n}$ , the correlation matrix is diagonalized as  $\langle \mathbf{n}_p \mathbf{n}_p^\dagger \rangle = \text{diag}\{\mathbf{0}_{1 \times 2M}, \mathbf{1}_{1 \times N-M}\}N_T$ . Therefore, using a detector that selectively separates such vectorial spaces, it would be possible to simultaneously transmit information signals and radiative heat without a reduction of the SNR.

In addition, since  $d_n = 1 \forall n$  and  $N > M$ , all noise signals exit through the right. In this case, the physical separation can be implemented by adding a network implementing the unitary transformation  $\mathbf{U}^\dagger$  [see Fig. 1(b)]. Such transformation changes the transfer matrix to  $\mathbf{T}_{\text{aux}} = \mathbf{I}_N \mathbf{D} \mathbf{V}^\dagger$ , where the basis for the output signals is given by the identity matrix, i.e., each output mode of the SVD decomposition is assigned to a physical port. We note that there are known algorithms for the

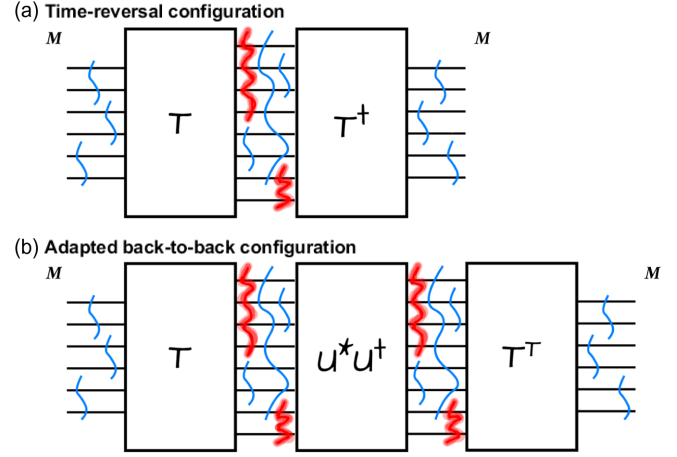


FIG. 2. (a) Time-reversal and (b) adapted back-to-back configurations.

design of optical networks implementing any arbitrary unitary transformation [54–57].

*Time-reversal processing*—The algebraic properties of CPA thermal noise signals also produce nontrivial heat transfer phenomena within time-reversal processing [58]. Let us assume that the aforementioned network is connected with a network characterized by transmission matrix  $\mathbf{T}^\dagger$  [see Fig. 2(a)], which effectively implements a time-reversal operator [58]. If the transmission matrix is unitary,  $\mathbf{T}^\dagger \mathbf{T} = \mathbf{I}_M$ , the network reproduces the input signals. However, one cannot generally expect  $\mathbf{T}^\dagger$  to be unitary for lossy networks, which generally fail to produce time-reversal operators.

However, for the time-reversal configuration (TR) depicted in Fig. 2(a), the resulting network is an  $M \times M$  network, characterized by scattering matrix  $\mathbf{S}_{\text{TR}} = \begin{bmatrix} \mathbf{0}_{M \times M} & \mathbf{T}_{\text{TR}}^T \\ \mathbf{T}_{\text{TR}} & \mathbf{0}_{M \times M} \end{bmatrix}$ . In this configuration, the transfer matrix is given by  $\mathbf{T}_{\text{TR}} = \mathbf{T}^\dagger \mathbf{T} = \mathbf{V} \mathbf{D}_T^2 \mathbf{V}^\dagger$ , which is now a positive semidefinite Hermitian matrix. Only if  $d_n = 1 \forall n$  we have that  $\mathbf{D}_T^2 = \mathbf{I}_M$  and the network recovers time-reversal processing. Interestingly, we note that even if  $d_n = 1 \forall n$  the network is still lossy, since it has  $N - M$  CPA channels, but it nevertheless performs time-reversal processing.

Again, the thermal noise signals exiting the network are characterized by the noise correlation matrix, which is given by (see Supplemental Material)  $\langle \mathbf{nn}^\dagger \rangle = \mathbf{P}_{\text{TR}} \mathbf{D}_{\text{TR}} \mathbf{P}_{\text{TR}}^\dagger N_T$  with

$$\mathbf{P}_{\text{TR}} = \begin{bmatrix} \mathbf{V}^* & \mathbf{0}_{M \times M} \\ \mathbf{0}_{M \times M} & \mathbf{V} \end{bmatrix} \quad (8)$$

and

$$\mathbf{D}_{\text{TR}} = \text{diag}\{1 - d_1^4, \dots, 1 - d_M^4, 1 - d_1^4, \dots, 1 - d_M^4\}. \quad (9)$$

It is clear from (9) that the thermal signals of the  $N - M$  CPA channels do not exit the network and are perfectly

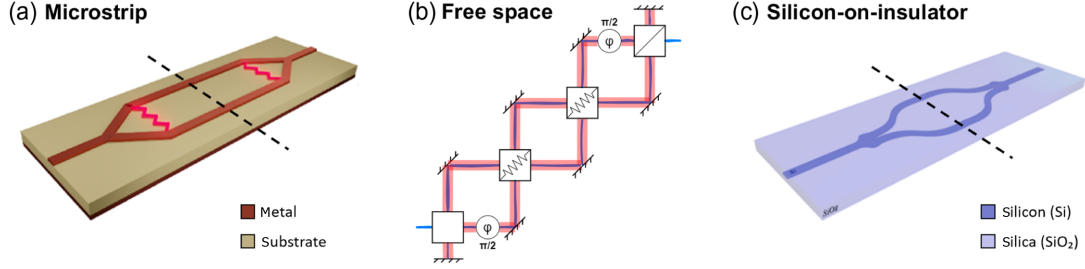


FIG. 3. Examples of time-reversal configurations based on two Wilkinson power dividers (WPDs) implemented in (a) microstrip, (b) free space and, (c) silicon-on-insulator technologies.

contained within the device. In fact, if the  $M$  modes are fully transparent, i.e.,  $d_n = 1 \forall n$ , no thermal signal would be observed outside the network. At the same time, there are CPA thermal signals flowing in the network, which lead to observable phenomena. If the two subnetworks are at temperature  $T_1$  and  $T_2$ , respectively, the net flux of radiative thermal between the two subnetworks would be  $P_{\text{th}} = (N - M)(N_{T_1} - N_{T_2})$ . Therefore, the properties of CPA modes enable the thermal radiative transmission of energy within a network, while it remains noiseless and transparent from the outside.

*Back-to-back configuration*—It must be noted that time reversal is not a simple back-to-back configuration, since the latter is characterized by a transmission matrix  $\mathbf{T}^T$  instead of  $\mathbf{T}^\dagger$ . Therefore, unless all elements of  $\mathbf{T}$  are real, the back-to-back configuration presents a different response from the time-reversal configuration. For example, a back-to-back configuration does not trap all CPA thermal noise signals within the network.

However, the trapping of CPA thermal noise signals can be recovered by introducing a matching network that performs the unitary transformation  $\mathbf{U}_c = \mathbf{U}^* \mathbf{U}^\dagger$  [see Fig. 2(b)]. Such network changes the basis of the output and input channels of  $\mathbf{T}$  and  $\mathbf{T}^T$ , respectively, so that they match, in what can be called an “adapted back-to-back” (aBB) configuration.

For such aBB configuration, the resulting network is an  $M \times M$  network characterized by the scattering matrix  $\mathbf{S}_{\text{aBB}} = [\mathbf{0}_{M \times M} \mathbf{T}_{\text{aBB}}^T; \mathbf{T}_{\text{aBB}} \mathbf{0}_{M \times M}]$ , where the transfer matrix is  $\mathbf{T}_{\text{aBB}} = \mathbf{T}^T \mathbf{U}_c \mathbf{T} = \mathbf{V}^* \mathbf{D}_T^2 \mathbf{V}^\dagger$  (see Supplemental Material). In this case, if  $d_n = 1 \forall n$ , we have that the transmission matrix reduces to  $\mathbf{T}_{\text{aBB}} = \mathbf{V}^* \mathbf{V}^\dagger$ , which is not necessarily the identity matrix. Thus, we find that the property of heat exchange mediated by CPA thermal channels, is not restricted to time-reversal processing and it is compatible with more arbitrary unitary transformations.

For the aBB configuration, the correlation matrix is given by (see Supplemental Material)  $\langle \mathbf{nn}^\dagger \rangle = \mathbf{P}_{\text{aBB}} \mathbf{D}_{\text{aBB}} \mathbf{P}_{\text{aBB}}^\dagger N_T$  with

$$\mathbf{P}_{\text{aBB}} = \begin{bmatrix} \mathbf{V}^* & \mathbf{0}_{M \times M} \\ \mathbf{0}_{M \times M} & \mathbf{V}^* \end{bmatrix} \quad (10)$$

and  $\mathbf{D}_{\text{aBB}} = \mathbf{D}_{\text{TR}}$ .

These results confirm that this configuration also ensures the full containment of CPA thermal noise signals within the network.

*Examples of applicability*—The theoretical effects described above apply to general CPA networks, and it is expected that they can be observed in many of the CPA technologies currently under investigation [1–4,8–23,26,31–34,37,38]. Next, we present a few examples on how these effects emerge on some popular CPA devices. First, we consider a Wilkinson power divider (WPD) [59], i.e., a  $1 \times 2$  device featuring a single CPA channel that has been studied within the context of quantum state transformations [14]. The scattering matrix of a WPD is given exactly by Eq. (1), with transfer matrix  $\mathbf{T}_{\text{WPD}} = 1/\sqrt{2} \mathbf{1}_{2 \times 1}$ . In addition, all elements of the transmission matrix are all real, so that  $\mathbf{T}^T = \mathbf{T}^\dagger = 1$ , and the time-reversal and back-to-back configurations are identical. Therefore, in both time-reversal and back-to-back configurations the total network matrix ( $\mathbf{S}_T$ ) can be expressed as  $\mathbf{S}_T = [0 \ 1; 1 \ 0]$ .

It is clear from  $\mathbf{S}_T$  that the combined system is perfectly transparent and lossless, as it could be expected from a time-reversal processing configuration. Therefore, WPDs provide an example of lossy CPA networks that remain perfectly transparent to electromagnetic waves via time-reversal processing, while allowing for the simultaneous transfer of heat between two subnetworks.

This effect could be observed in a variety of technological platforms as illustrated in Fig. 3. First, WPDs have been traditionally implemented at microwave frequencies by using microstrip lines and resistors [see Fig. 3(a)]. They are routinely used in microwave networks, being a common component of beam-forming networks [60–62] and amplification stages [63,64]. In addition, generalizations to WPDs with arbitrary number of output ports and splitting ratios have been demonstrated [65]. In addition, Fig. 3(b) depicts an free-space optical setup where the WPDs are implemented with a combination of beam splitters, lossy beam splitters, and mirrors (see Supplemental Material for a theoretical description of the network). On the other hand, Fig. 3(c) shows a system implemented in integrated optics through silicon-on-insulator technology. In this case, modified  $Y$  branches can be used as WPDs [14].



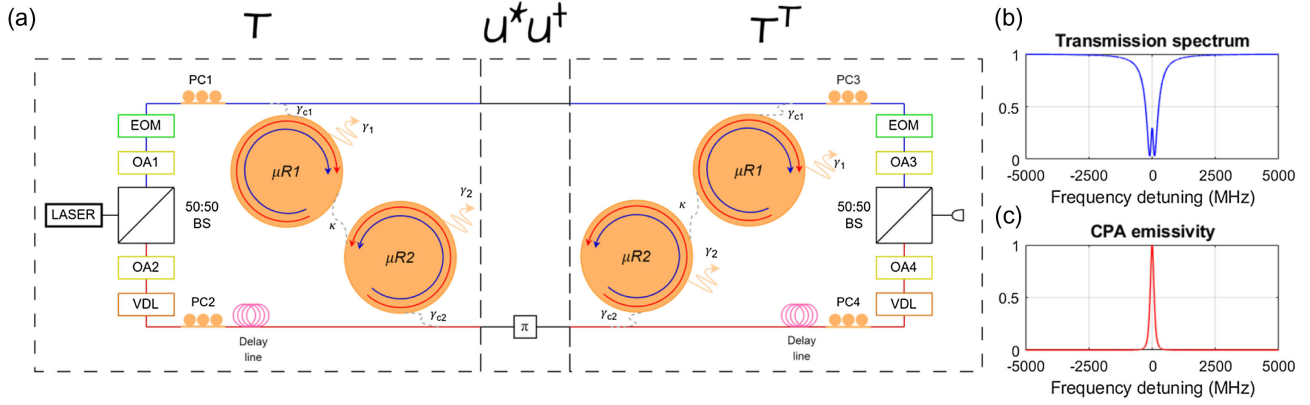


FIG. 4. (a) Example of an aBB configuration based on the system presented in [22]. (b) Transmitted signal and (c) internal heat transfer spectra. These results were obtained for the following parameters:  $\gamma_1 = 64.782$  MHz,  $\gamma_2 = 242.93$  MHz,  $\gamma_{c1} = 184.63$  MHz, and  $\gamma_{c2} = 123.09$  MHz, enforcing a generic CPA EP.

Finally, we present an example that does not operate in a TR configuration and presents filtering effects with a nontrivial dispersion profile, based on the recently studied CPA at an exceptional point (EP) [22]. The system [see Fig. 4(a)], consists of two silica microtoroidal resonators, coupled to two single-mode fiber conical waveguides. It is a very general platform that leads to different classes of EPs in function of the system parameters. We focus on the “Generic CPA EP,” for which two zeros converge on the real axis, forming an EP with CPA properties. That is to say, two eigenvalues of the system are simultaneously zero and two eigenvectors coalesce to  $1/\sqrt{2}[1, i]$ .

As detailed in the Supplemental Material, an aBB can be constructed by using a unitary matrix  $U_c = U_G^* U_G^\dagger = \text{diag}\{1, -1\}$ , which can be easily implemented with a delay line [shown as a  $\pi$  block in Fig. 4(a)]. Figure 4(b) shows the transmission through the system when internal phase shifters are tuned to excite  $1/\sqrt{2}[1, -i]$  signals orthogonal to the EP eigenvalue. The transmission is characterized by an absorbing doublet. At the same time, the internal emissivity associated with the EP eigenvector  $1/\sqrt{2}[1, i]$  presents a single peak at the EP frequency [see Fig. 4(c)]. At this point, CPA signals are transferred between both resonator networks, with unit efficiency, without disturbing the transmitted signals. If the resonator loss were dissipative, this mechanism would allow for heat transfer between both resonator systems. If the losses were predominantly radiative, such channel would allow the coupling of external signals through the resonators. This example shows that it is possible to implement filtering with a nontrivial dispersion profile, while simultaneously enabling heat transfer between two subnetworks that does not increase the externally observable noise.

**Conclusions**—Our results demonstrate that CPA thermal noise signals have a singular property: they are orthogonal to the signals transmitted through the network. This property can be understood as a form of spatial coherence, which enables the physical separability of CPA thermal

noise signals via networks implementing unitary transformations. In addition, such property can be harnessed in time-reversal and adapted back-to-back configurations, enabling heat transfer channels that remain confined within the network, and thus do not increase the externally observable noise. In general, we believe that our results highlight the nontrivial thermal noise properties of CPA, which remain relatively unexplored. CPA wave phenomena are being currently investigated in a large number of technological platforms [1–4, 8–23, 26, 31–38], and we believe that our results present a new perspective in which to look and reexamine CPA systems.

**Acknowledgments**—I.L. acknowledges support from Ramón y Cajal fellowship RYC2018-024123-I by MCIU/AEI/FEDER/UE, and ERC Starting Grant No. 948504. D.O. acknowledges support from UPNA-RyC predoctoral fellowships.

- [1] Y. D. Chong, L. Ge, H. Cao, and A. D. Stone, Coherent perfect absorbers: Time-reversed lasers, *Phys. Rev. Lett.* **105**, 053901 (2010).
- [2] J. Zhang, K. F. MacDonald, and N. I. Zheludev, Controlling light-with-light without nonlinearity, *Light Sci. Appl.* **1**, e18 (2012).
- [3] D. G. Baranov, A. Krasnok, T. Shegai, A. Alù, and Y. Chong, Coherent perfect absorbers: Linear control of light with light, *Nat. Rev. Mater.* **2**, 17064 (2017).
- [4] L. Ge, Y. D. Chong, and A. D. Stone, Steady-state *ab initio* laser theory: Generalizations and analytic results, *Phys. Rev. A* **82**, 063824 (2010).
- [5] W. R. Sweeney, C. W. Hsu, and A. D. Stone, Theory of reflectionless scattering modes, *Phys. Rev. A* **102**, 063511 (2020).
- [6] A. D. Stone, W. R. Sweeney, C. W. Hsu, K. Wisal, and Z. Wang, Reflectionless excitation of arbitrary photonic structures: A general theory, *Nanophotonics* **10**, 343 (2020).

- [7] J. Sol, A. Alhulaymi, A. D. Stone, and P. Del Hougne, Reflectionless programmable signal routers, *Sci. Adv.* **9**, eadf0323 (2023).
- [8] W. Wan, Y. Chong, L. Ge, H. Noh, A. D. Stone, and H. Cao, Time-reversed lasing and interferometric control of absorption, *Science* **331**, 889 (2011).
- [9] W. Zhu, F. Xiao, M. Kang, and M. Premaratne, Coherent perfect absorption in an all-dielectric metasurface, *Appl. Phys. Lett.* **108**, 121901 (2016).
- [10] S. M. Rao, J. J. Heitz, T. Roger, N. Westerberg, and D. Faccio, Coherent control of light interaction with graphene, *Opt. Lett.* **39**, 5345 (2014).
- [11] A. Espinosa-Soria, E. Pinilla-Cienfuegos, F. J. Díaz-Fernández, A. Griol, J. Martí, and A. Martínez, Coherent control of a plasmonic nanoantenna integrated on a silicon chip, *ACS Photonics* **5**, 2712 (2018).
- [12] R. Bruck and O. L. Muskens, Plasmonic nanoantennas as integrated coherent perfect absorbers on SOI waveguides for modulators and all-optical switches, *Opt. Express* **21**, 27652 (2013).
- [13] S. Zanotto, F. Bianco, V. Miseikis, D. Convertino, C. Coletti, and A. Tredicucci, Coherent absorption of light by graphene and other optically conducting surfaces in realistic on-substrate configurations, *APL Photonics* **2**, 016101 (2017).
- [14] O. Hernández, A. Ortega-Gomez, M. Bravo, and I. Liberal, Quantum interference in Wilkinson power dividers, *Laser Photonics Rev.* **16**, 2200095 (2022).
- [15] M. J. Jung, C. Han, J. W. Yoon, and S. H. Song, Temperature and gain tuning of plasmonic coherent perfect absorbers, *Opt. Express* **23**, 19837 (2015).
- [16] J. Luo, B. Liu, Z. H. Hang, and Y. Lai, Coherent perfect absorption via photonic doping of zero-index media, *Laser Photonics Rev.* **12**, 1800001 (2018).
- [17] T. Roger, S. Vezzoli, E. Bolduc, J. Valente, J. J. Heitz, J. Jeffers, C. Soci, J. Leach, C. Couteau, N. I. Zheludev *et al.*, Coherent perfect absorption in deeply subwavelength films in the single-photon regime, *Nat. Commun.* **6**, 7031 (2015).
- [18] A. N. Vetlugin, R. Guo, A. Xomalis, S. Yanikgonul, G. Adamo, C. Soci, and N. I. Zheludev, Coherent perfect absorption of single photons in a fiber network, *Appl. Phys. Lett.* **115**, 191101 (2019).
- [19] A. N. Vetlugin, Coherent perfect absorption of quantum light, *Phys. Rev. A* **104**, 013716 (2021).
- [20] O. Hernández and I. Liberal, Generalized approach to quantum interference in lossy n-port devices via a singular value decomposition, *Opt. Express* **30**, 31267 (2022).
- [21] K. Pichler, M. Kühmayer, J. Böhm, A. Brandstötter, P. Ambichl, U. Kuhl, and S. Rotter, Random anti-lasing through coherent perfect absorption in a disordered medium, *Nature (London)* **567**, 351 (2019).
- [22] C. Wang, W. R. Sweeney, A. D. Stone, and L. Yang, Coherent perfect absorption at an exceptional point, *Science* **373**, 1261 (2021).
- [23] X. Jiang, S. Yin, H. Li, J. Quan, H. Goh, M. Cotrufo, J. Kullig, J. Wiersig, and A. Alù, Coherent control of chaotic optical microcavity with reflectionless scattering modes, *Nat. Phys.* **20**, 109 (2023).
- [24] C. Ferise, P. Del Hougne, S. Félix, V. Pagneux, and M. Davy, Exceptional points of  $PT$ -symmetric reflectionless states in complex scattering systems, *Phys. Rev. Lett.* **128**, 203904 (2022).
- [25] J. Sol, M. Röntgen, and P. del Hougne, Covert scattering control in metamaterials with non-locally encoded hidden symmetry, *Adv. Mater.* **36**, 2303891 (2024).
- [26] Y. Slobodkin, G. Weinberg, H. Hörner, K. Pichler, S. Rotter, and O. Katz, Massively degenerate coherent perfect absorber for arbitrary wavefronts, *Science* **377**, 995 (2022).
- [27] M. F. Imani, D. R. Smith, and P. del Hougne, Perfect absorption in a disordered medium with programmable meta-atom inclusions, *Adv. Funct. Mater.* **30**, 2005310 (2020).
- [28] B. W. Frazier, T. M. Antonsen Jr, S. M. Anlage, and E. Ott, Wavefront shaping with a tunable metasurface: Creating cold spots and coherent perfect absorption at arbitrary frequencies, *Phys. Rev. Res.* **2**, 043422 (2020).
- [29] P. del Hougne, K. B. Yeo, P. Besnier, and M. Davy, On-demand coherent perfect absorption in complex scattering systems: Time delay divergence and enhanced sensitivity to perturbations, *Laser Photonics Rev.* **15**, 2000471 (2021).
- [30] P. Del Hougne, K. B. Yeo, P. Besnier, and M. Davy, Coherent wave control in complex media with arbitrary wavefronts, *Phys. Rev. Lett.* **126**, 193903 (2021).
- [31] A. Müllers, B. Santra, C. Baals, J. Jiang, J. Benary, R. Labouvie, D. A. Zezyulin, V. V. Konotop, and H. Ott, Coherent perfect absorption of nonlinear matter waves, *Sci. Adv.* **4**, 6539 (2018).
- [32] C. Meng, X. Zhang, S. T. Tang, M. Yang, and Z. Yang, Acoustic coherent perfect absorbers as sensitive null detectors, *Sci. Rep.* **7**, 43574 (2017).
- [33] J. Sol, D. R. Smith, and P. Del Hougne, Meta-programmable analog differentiator, *Nat. Commun.* **13**, 1713 (2022).
- [34] M. Papaioannou, E. Plum, J. Valente, E. T. Rogers, and N. I. Zheludev, All-optical multichannel logic based on coherent perfect absorption in a plasmonic metamaterial, *APL Photonics* **1**, 090801 (2016).
- [35] S. F. Liew, S. M. Popoff, S. W. Sheehan, A. Goetschy, C. A. Schmuttenmaer, A. D. Stone, and H. Cao, Coherent control of photocurrent in a strongly scattering photoelectrochemical system, *ACS Photonics* **3**, 449 (2016).
- [36] G. Pirruccio, M. Ramezani, S. R.-K. Rodriguez, and J. G. Rivas, Coherent control of the optical absorption in a plasmonic lattice coupled to a luminescent layer, *Phys. Rev. Lett.* **116**, 103002 (2016).
- [37] J. Erb, D. Shrekenhamer, T. Sleasman, T. M. Antonsen, and S. M. Anlage, Control of the scattering properties of complex systems by means of tunable metasurfaces, *Acta Phys. Pol. A* **144**, 421 (2023).
- [38] F. S. Cuesta, A. D. Kuznetsov, G. A. Ptitcyn, X. Wang, and S. A. Tretyakov, Coherent asymmetric absorbers, *Phys. Rev. Appl.* **17**, 024066 (2022).
- [39] T. Gruner and D.-G. Welsch, Quantum-optical input-output relations for dispersive and lossy multilayer dielectric plates, *Phys. Rev. A* **54**, 1661 (1996).
- [40] J. Jeffers, Nonlocal coherent perfect absorption, *Phys. Rev. Lett.* **123**, 143602 (2019).

- [41] S. Wijewardane and D. Goswami, A review on surface control of thermal radiation by paints and coatings for new energy applications, *Renewable Sustainable Energy Rev.* **16**, 1863 (2012).
- [42] E. Ring and K. Ammer, Infrared thermal imaging in medicine, *Physiol. Meas.* **33**, R33 (2012).
- [43] M. R. Watts, M. J. Shaw, and G. N. Nielson, Microphotonic thermal imaging, *Nat. Photonics* **1**, 632 (2007).
- [44] Y. Qu, Q. Li, L. Cai, M. Pan, P. Ghosh, K. Du, and M. Qiu, Thermal camouflage based on the phase-changing material GST, *Light Sci. Appl.* **7**, 26 (2018).
- [45] S. Hong, S. Shin, and R. Chen, An adaptive and wearable thermal camouflage device, *Adv. Funct. Mater.* **30**, 1909788 (2020).
- [46] N. Li, H. Yuan, L. Xu, J. Tao, D. K. T. Ng, L. Y. T. Lee, D. D. Cheam, Y. Zeng, B. Qiang, Q. Wang *et al.*, Radiation enhancement by graphene oxide on microelectromechanical system emitters for highly selective gas sensing, *ACS Sens.* **4**, 2746 (2019).
- [47] N. A. Karker, G. Dharmalingam, and M. A. Carpenter, Thermal energy harvesting near-infrared radiation and accessing low temperatures with plasmonic sensors, *Nanoscale* **7**, 17798 (2015).
- [48] See Supplemental Material at <http://link.aps.org/supplemental/10.1103/PhysRevLett.133.103801> for extended details on the theoretical derivations and additional examples.
- [49] D. A. Miller, All linear optical devices are mode converters, *Opt. Express* **20**, 23985 (2012).
- [50] H. A. Haus, Optimum noise performance of optical amplifiers, *IEEE J. Quantum Electron.* **37**, 813 (2001).
- [51] L. Zhu, S. Sandhu, C. Otey, S. Fan, M. B. Sinclair, and T. Shan Luk, Temporal coupled mode theory for thermal emission from a single thermal emitter supporting either a single mode or an orthogonal set of modes, *Appl. Phys. Lett.* **102**, 103104 (2013).
- [52] D. A. Miller, L. Zhu, and S. Fan, Universal modal radiation laws for all thermal emitters, *Proc. Natl. Acad. Sci. U.S.A.* **114**, 4336 (2017).
- [53] J.-J. Greffet, P. Bouchon, G. Bruccoli, and F. Marquier, Light emission by nonequilibrium bodies: Local kirchhoff law, *Phys. Rev. X* **8**, 021008 (2018).
- [54] M. Reck, A. Zeilinger, H. J. Bernstein, and P. Bertani, Experimental realization of any discrete unitary operator, *Phys. Rev. Lett.* **73**, 58 (1994).
- [55] D. A. Miller, Self-configuring universal linear optical component, *Photonics Res.* **1**, 1 (2013).
- [56] S. Pai, B. Bartlett, O. Solgaard, and D. A. B. Miller, Matrix optimization on universal unitary photonic devices, *Phys. Rev. Appl.* **11**, 064044 (2019).
- [57] M. Moralis-Pegios, G. Giamougiannis, A. Tsakyridis, D. Lazovsky, and N. Pleros, Perfect linear optics using silicon photonics, *Nat. Commun.* **15**, 5468 (2024).
- [58] M. Tanter, J.-L. Thomas, and M. Fink, Time reversal and the inverse filter, *J. Acoust. Soc. Am.* **108**, 223 (2000).
- [59] D. M. Pozar, *Microwave Engineering* (John Wiley & Sons, New York, 2011).
- [60] V. Ruchonkov, V. Teplyakov, and A. Petrov, Implementation of antenna array beamforming networks designed on Wilkinson bridges, *J. Commun. Technol. Electron.* **63**, 342 (2018).
- [61] T. Albuquerque, T. Silva, A. Serres, R. Freire, J. Walheim, F. Podevin, F. Burdin, P. Ferrari, and T. Vuong, Implementation of beam-steering front-ends at 2.45 GHz using modified Wilkinson power dividers, reflexion type phase shifters and c-shape monopole antennas: First results, in *Proceedings of the 2015 SBMO/IEEE MTT-S International Microwave and Optoelectronics Conference (IMOC)* (IEEE, New York, 2015), pp. 1–5.
- [62] C. Biurrun-Quel and C. Del-Río Bocio, Studying the noise performance of corps beam forming networks, in *Proceedings of the 2022 16th European Conference on Antennas and Propagation (EuCAP)* (2022), pp. 1–5.
- [63] R. Gatti, M. Dionigi, and R. Sorrentino, Computation of gain, noise figure, and third-order intercept of active array antennas, *IEEE Trans. Antennas Propag.* **52**, 3139 (2004).
- [64] J. Lee, G/t and noise figure of active array antennas, *IEEE Trans. Antennas Propag.* **41**, 241 (1993).
- [65] J.-L. Li and B.-Z. Wang, Novel design of Wilkinson power dividers with arbitrary power division ratios, *IEEE Transactions on Industrial Electronics* **58**, 2541 (2011).